



HAL
open science

Patient-Specific Computational Evaluation of Stiffness Distribution in Ascending Thoracic Aortic Aneurysm

Marzio Di Giuseppe, Solmaz Farzaneh, Massimiliano Zingales, Salvatore Pasta, Stéphane Avril

► **To cite this version:**

Marzio Di Giuseppe, Solmaz Farzaneh, Massimiliano Zingales, Salvatore Pasta, Stéphane Avril. Patient-Specific Computational Evaluation of Stiffness Distribution in Ascending Thoracic Aortic Aneurysm. *Journal of Biomechanics*, inPress, pp.110321. 10.1016/j.jbiomech.2021.110321 . hal-03139856

HAL Id: hal-03139856

<https://hal.science/hal-03139856v1>

Submitted on 12 Feb 2021

HAL is a multi-disciplinary open access archive for the deposit and dissemination of scientific research documents, whether they are published or not. The documents may come from teaching and research institutions in France or abroad, or from public or private research centers.

L'archive ouverte pluridisciplinaire **HAL**, est destinée au dépôt et à la diffusion de documents scientifiques de niveau recherche, publiés ou non, émanant des établissements d'enseignement et de recherche français ou étrangers, des laboratoires publics ou privés.

1 **Patient-Specific Computational Evaluation of Stiffness Distribution in Ascending**
2 **Thoracic Aortic Aneurysm**

3 Marzio Di Giuseppe¹, Solmaz Farzaneh², Massimiliano Zingales³,
4 Salvatore Pasta³, Stéphane Avril²

5
6
7 ¹ Department of Health Promotion, Mother and Child Care, Internal Medicine and Medical
8 Specialties, University of Palermo, 90128, Palermo, Italy

9 ² Mines Saint-Etienne, Univ Lyon, Univ Jean Monnet, INSERM, U1059 SAINBIOSE, Saint-
10 Étienne, 42023, France

11 ³ Department of Engineering, Viale delle Scienze, Ed.8, University of Palermo, 90128,
12 Palermo, Italy

13
14
15
16
17
18 Submitting for Original Article

19
20
21
22 Manuscript word count: 3360 words

23
24
25
26 Corresponding author:

27 Stéphane Avril
28 Univ Lyon, INSERM U1059,
29 Mines Saint-Etienne, SAINBIOSE, F-42023,
30 158 cours Fauriel,
31 42023 SAINT-ETIENNE cedex 2, France
32 Phone: +33477420188
33 Fax : +33477420000
34 Email: avril@emse.fr

35
36
37
38
39
40
41
42
43
44
45
46
47
48
49
50
51
52
53
54
55
56
57
58
59
60
61
62

Abstract

Quantifying local aortic stiffness properties in vivo is acknowledged as essential to assess the severity of an ascending thoracic aortic aneurysm (ATAA). Recently, the LESI (local extensional stiffness identification) methodology has been established to quantify non-invasively local stiffness properties of ATAAs using electrocardiographic-gated computed tomography (ECG-gated CT) scans. The aim of the current study was to determine the most sensitive markers of local ATAA stiffness estimation with the hypothesis that direct measures of local ATAA stiffness could better detect the high-risk patients.

A cohort of 30 patients (12 BAV and 18 TAV) referred for aortic size evaluation by ECG-gated CT were recruited. For each patient, the extensional stiffness Q was evaluated by the LESI methodology whilst computational flow analyses were also performed to derive hemodynamics markers such as the wall shear stress (WSS).

A strong positive correlation was found between the extensional stiffness and the aortic pulse pressure ($R=0.644$ and $p<0.001$). Interestingly, a significant positive correlation was also found between the extensional stiffness and patients age for BAV ATAAs ($R=0.619$ and $p=0.032$), but not for TAV ATAAs ($R=-0.117$ and $p=0.645$). No significant correlation was found between the extensional stiffness and WSS evaluated locally. There was no significant difference either in the extensional stiffness between BAV ATAAs and TAV ATAAs ($Q=3.6\pm 2.5$ MPa.mm for BAV ATAAs vs $Q=5.3\pm 3.1$ MPa.mm for TAV ATAAs, $p=0.094$).

Future work will focus on relating the extensional stiffness to the patient-specific rupture risk of ATAAs on larger cohorts to confirm the promising interest of the LESI methodology.

Keywords: Ascending Thoracic Aortic Aneurysm, Bicuspid Aortic Valve, Extensional Stiffness, Noninvasive Inverse Method, Shear Stress

63

64 **Introduction**

65 Ascending thoracic aortic aneurysm (ATAA) is a life-threatening cardiovascular disease,
66 leading to weakening of the aortic wall and permanent dilation. ATAA affects approximately
67 10 out of 100,000 persons per year in the general population (Coady et al., 1999), and this
68 disease is associated with a high risk of mortality and morbidity (Elefteriades and Farkas,
69 2010). Bicuspid aortic valve (BAV) is a predisposing risk factor to ATAA formation and
70 development with patients having associated aortopathy on approximately 40% of whole
71 bicuspid population (Verma and Siu, 2014) and higher rate of aortic dissection compared to
72 patients with the tricuspid aortic valve (TAV) (Januzzi et al., 2004).

73

74 To avoid aortic complications (i.e. rupture or dissection), the current clinical management of
75 ATAA is based on strict monitoring of the aneurysm size and elective repair is recommended
76 when aortic diameter reaches a critical size (Borger et al., 2018). However, aortic size is not
77 a sufficient predictor of the risk of ATAA failure (Pape et al., 2007). Aortic stiffness is
78 associated with progressive aortic dilatation and aneurysm formation as shown by imaging
79 modalities (Longobardo et al., 2017; Teixeira et al., 2012), computational analyses (Farzaneh
80 et al., 2019a; Martin et al., 2013a; Pasta et al., 2017a) and biomechanical studies (Selvin et
81 al., 2010; Smoljkic et al., 2017). High aortic stiffness was associated with high rates of
82 surgical aortic replacement and aortic root dilation in children and adults with connective
83 tissue disorders (Prakash et al., 2015). In Marfan patients, aortic stiffness proved to be
84 important in predicting progressive aortic dilatation (Guala et al., 2019; Sulejmani et al.,
85 2017). A recent study of abdominal aortic aneurysms found that segmental stiffening of the
86 aorta preceded aneurysm growth and introduced the concept that stiffening may act as an
87 early mechanism triggering elastin breakdown and aneurysm growth (Raaz et al., 2015).
88 Imaging based on 4D Flow MRI (Mahadevia et al., 2014), in silico computational modeling
89 (Mendez et al., 2018; Pasta et al., 2017b) or combination of them (Youssefi et al., 2017)
90 have confirmed an altered hemodynamic environment in BAV ATAAs with well-functioning or

91 stenotic aortic valve leaflets (van Ooij et al., 2017). The underlying hypothesis is that flow
92 disturbances induce local wall shear stress (WSS) forces on the dilated aorta, portending to
93 adverse vascular remodeling by mechanotransduction. This can further lead to changes in
94 the biomechanical properties of ATAA wall as reflected by an increased stiffness for the
95 dilated aorta.

96

97 Risk assessment based on the aortic stiffness of the ATAA wall are being developed (Duprey
98 et al., 2016; Farzaneh et al., 2019b; Martin et al., 2013a). In this way, the quantification of
99 local elastic properties of the ATAA wall from in vivo data is crucial to establish a reliable
100 method for estimating the severity of an ATAA (Mousavi and Avril, 2017; Rooprai et al.,
101 2019). Most importantly, new strategies of risk assessment should be accurate and
102 compatible with clinical time framework. For that purpose, the in vivo non-invasive
103 identification of aortic stiffness would be essential for clinicians to improve the clinical
104 decision making process. Recently, Farzaneh et al. (Farzaneh et al., 2019a) have presented
105 a novel methodology, namely the LESI (local extensional stiffness identification)
106 methodology, to non-invasively quantify local stiffness properties on the basis of ECG-gated
107 CT scans and brachial arm pressure. The interrelationship between the obtained local
108 stiffness with other established markers of aortic function remains unclear and this currently
109 limits the methodology's potential impact. The aim of the current study was to determine the
110 most sensitive markers of local ATAA stiffness estimation with the hypothesis that direct
111 measures of local ATAA stiffness could better detect the high-risk patients. First, the patterns
112 of extensional stiffness obtained by the LESI methodology in a cohort of 30 patients with
113 ATAAs and different aortic valve phenotypes were analyzed. Then, the association of
114 stiffness with demographic data and computationally derived wall shear stress (WSS) was
115 investigated.

116

117

118

119

120 **Methods**

121 ***Study Population***

122 After internal review board approval and informed consent, 30 patients (12 BAV and 18 TAV)
123 referred for aortic size evaluation by electrocardiographic-gated computed tomography
124 (ECG-gated CT) were enrolled. Table 1 shows demographic data of the patient population as
125 well as aortic diameter. For all patients, ECG-gated CT scans were performed after
126 intravenous injection of contrast agent to improve image quality. Imaging was carried out on
127 a GE VCT 64-channel scanner (GE Medical Systems, Milwaukee, Wisconsin), with gantry
128 rotation velocity of 0.5 m/s and spiral pitch of 0.984. Retrospective reconstruction of images
129 was performed to obtain images at cardiac phases corresponding to both end-diastole and
130 end-systole at the resolution of 512 x 512 and slice thickness of 0.625 mm. Prior to imaging,
131 diastolic and systolic blood pressures were measured by brachial sphygmomanometer for
132 each patient.

133

134 ***Images Analysis***

135 For each patient, segmentation of ECG-gated CT images was performed at both diastolic
136 and systolic phases using Mimics v20 (Materialise, Leuven, BE). Specifically, semi-automatic
137 threshold-based segmentation of the aortic lumen was performed to obtain a point cloud of
138 ATAA geometries. The same smoothing factor was applied to all phases. The three-
139 dimensional (3D) surface of the aorta was generated for each phase and exported as STL
140 file. Then, 3D aortic surfaces reconstructed at both cardiac phases were cut by identical
141 cross-sectional planes in Rhinoceros (Robert McNeel & Associates, Seattle, USA) to define a
142 domain of the aorta larger than the final segment of interest. A set of nodes was defined
143 across each reconstructed aortic geometry, with the requirement that a node represented the
144 position of the same material point at each phase of the cardiac cycle. For this, it was
145 essential to reconstruct a structural mesh for all phases with an identical number of elements
146 and nodes. The Vascular Modeling Toolkit (VMTK, Orobix, Bergamo, Italy; www.vmtk.org)

147 (Antiga and Steinman, 2004) was employed to generate the structural mesh from STL files.
 148 The extracted data from VMTK were postprocessed in MATLAB to extract an accurate mesh
 149 using the longitudinal and circumferential metrics obtained from VMTK. A structural mesh
 150 composed of 3871 quadrilateral shell elements, 49 along the circumferential direction and 79
 151 along the longitudinal direction, was defined on the template geometry. Each node of the
 152 structural mesh was related to assumedly the same material points for systole and diastole
 153 phases.

154 The LESI methodology for calculating the extensional stiffness was described by Farzaneh et
 155 al. (Farzaneh et al., 2019a). In brief, local principal strain components (ε_1 and ε_2) were
 156 deduced by computing the spatial gradients of displacements between diastolic and systolic
 157 configurations. Although the aortic tissue is globally anisotropic and nonlinear, its mechanical
 158 behavior was linearized in the range of strains induced by pressure variations between
 159 diastole and systole, and anisotropic effects were neglected in this range. The local principal
 160 stress components (τ_1^0 and τ_2^0) were derived by finite-element analysis (FEA) performed on
 161 the ATAA diastolic geometry using average blood pressure evaluated over the cardiac cycle
 162 (Joldes et al., 2016). To obtain radii of curvature (r_1^0 and r_2^0) and their variations (Δr_2 and Δr_1)
 163 fast and efficiently, a method based on the principle of virtual work was developed, as
 164 previously introduced in Bersi et al. (Bersi et al., 2016).

165 Finally it was possible, for each element, to relate the extensional stiffness to the pulsed
 166 pressure ΔP such as:

$$167 \quad Q = \frac{\Delta P + \frac{\tau_1^0 \Delta r_1}{(r_1^0)^2} + \frac{\tau_2^0 \Delta r_2}{(r_2^0)^2}}{\frac{\varepsilon_1 + \nu \varepsilon_2}{r_1^0} + \frac{\nu \varepsilon_1 + \varepsilon_2}{r_2^0}}$$

168 In the current study we used the concept of “extensional stiffness” (intensive property) which
 169 equals the material stiffness times the thickness and whose dimension is MPa.mm.

170 The aortic thickness could not be measured accurately due to the limited spatial resolution of
 171 CT.

172 Once LESI results were obtained for each patient, the average extensional stiffness was
173 evaluated in each of the four quadrants, including the major, minor, anterior and posterior
174 regions (Fig.1).

175

176 ***Computational Flow Analysis***

177 Computational flow modeling was applied to study ATAA hemodynamics at systolic peak
178 when the aortic valve is supposedly fully open (D'Ancona et al., 2013). For each patient, the
179 fluid domain of ATAA geometry at end-systole was meshed with unstructured tetrahedral
180 elements with size of 0.1 mm. The blood was assumed as a non-Newtonian incompressible
181 fluid (density of 1060 kg/m³ and viscosity of 0.00371 Pa*s) adopting the Carreau model
182 (Khanafar et al., 2006; Leuprecht and Perktold, 2001). The solution was obtained with
183 FLUENT v18 (ANSYS Inc., Canonsburg, PA) using the SIMPLE algorithm for the pressure-
184 velocity coupling and second order accurate discretization scheme. To include patient-
185 specific hemodynamics conditions, the transaortic jet velocity evaluated by Doppler
186 echocardiography was set as the inflow velocity condition at the aortic valve plane. For each
187 outlet, we first computed the global vascular resistance and arterial compliance of each
188 patient from echocardiographic measurements and clinical demographic data. Then, these
189 parameters were used to compute the outflow boundary conditions of a three-element
190 Windkessel model (comprising proximal resistance, compliance, and a distal resistance)
191 coupled to each outflow branch. Boundary conditions were adjusted to match brachial artery
192 pulse pressure.

193 After numerical solution, WSS values were obtained for the entire thoracic aorta, with further
194 in-depth subanalysis in the ascending thoracic aorta by computing maxima at sinotubular
195 junction (namely, analysis plane = AA1), proximal (AA2) and mid (AA3) ascending thoracic
196 aorta for each quadrant (i.e., major, minor, anterior and posterior quadrants).

197

198

199

200 **Statistical Analysis**

201 The Rank Sum test was used to assess differences in the extensional stiffness between BAV
202 ATAAs and TAV ATAAs. One-way Anova, followed by Holm-Sidak post-hoc test for all pair-
203 wise comparisons, was used to assess differences of extensional stiffness among aortic
204 quadrants. The association of the extensional stiffness with patient age, aortic pulse
205 pressure, aortic diameter, WSS, aortic strain and stress was explored by Pearson's
206 correlation. Statistical analyses were performed using SigmaPlot (Systat Software Inc., San
207 Jose, California), with statistical significance set at $p=0.05$ in all cases. Data are shown as
208 Mean \pm SEM.

209
210 In addition, Principal Component Analysis (PCA) was performed for dimensionality reduction
211 of all data computed for each patient. First two principal components were analyzed to
212 assess separation of BAV ATAA versus TAV ATAA. The tolerance ellipse based on
213 Hotelling's T2 at a significance level of 0.05 was calculated and shown in the score plots.
214 Principal Component Analysis was performed using SPSS software (IBM SPSS Statistics
215 v.17, New York, NY).

216

217 **Results**

218 Table 1 summarizes patient demographic data, systolic and diastolic pressures and aortic
219 diameter. The distribution of age in BAV ATAAs differs significantly from that of TAV ATAAs
220 patients (50.2 ± 7.5 years for BAV ATAAs vs 64.7 ± 7.8 years for TAV ATAAs, $p<0.01$), and
221 this difference was confirmed by the analysis of the age on a different cohort of 159 patients
222 (Agnese et al., 2019).

223

224 Fig. 2 and Fig. 3 show representative extensional stiffness and WSS maps obtained by the
225 LESI methodology and CFD analyses for BAV ATAAs and TAV ATAAs, respectively. There
226 was no significant difference in the extensional stiffness (Q) between BAV ATAAs and TAV
227 ATAAs ($Q=3.6\pm 2.5$ MPa.mm for BAV ATAAs vs $Q=5.3\pm 3.1$ MPa.mm for TAV ATAAs,

228 p=0.094). Similarly, the mean values of the extensional stiffness did not significantly change
229 among aortic quadrants (see Fig.4), although many patients had high values of the
230 extensional stiffness in the minor and anterior quadrants of the ascending aorta.

231

232 The relationship of extensional stiffness as averaged among quadrants with the ascending
233 aortic diameter and the aortic pulse pressure are shown in Fig.5A and Fig.5B. A strong
234 positive correlation was found between the extensional stiffness and the aortic pulse
235 pressure ($R=0.644$ and $p<0.001$), but was not significant between the extensional stiffness
236 and the aortic diameter ($R=0.341$ and $p=0.065$). Interestingly, a significant positive
237 correlation was found between extensional stiffness and patients age for BAV ATAAs
238 ($R=0.619$ and $p=0.032$), but not for TAV ATAAs ($R=-0.117$ and $p=0.645$) as shown by
239 Fig. 5C and Fig. 5D. Fig. 5E and Fig. 5F show the relationship of both strain and stress
240 obtained in the circumferential direction with the average extensional stiffness. The
241 extensional stiffness was inversely correlated with the circumferential strain ($R=-0.522$ and
242 $p=0.00324$) and positively with the circumferential stress ($R=0.474$ and $p=0.008$). Correlation
243 analysis of extensional stiffness with age (Fig.5C) also revealed that BAV ATAAs can be
244 divided into two subgroups: 1) patients younger than 50 years old who had a relatively low
245 extensional stiffness, 2) patients older than 55 years old who had a relatively high
246 extensional stiffness. All analysis in Fig.5 were also broken down by aneurysm type, results
247 are reported in Fig.A1.

248

249 Peak systolic WSSs were correlated to the average extensional stiffness for each ascending
250 aortic level and aortic quadrant. The correlation analysis between extensional stiffness and
251 WSS values evaluated at proximal ascending thoracic aorta (AA2) appears promising
252 ($R=0.343$ and $p=0.080$ for AA2), but no significant correlation was found between stiffness and
253 WSS evaluated locally for Major, Minor and Anterior quadrants. For the Posterior quadrant a
254 correlation was identified although the obtained p-value was very close to the threshold

255 ($p=0.05$) and a low coefficient was obtained. Results are presented in Fig.6. All analysis were
256 also broken down by aneurysm type, results are reported in Fig.A2.

257

258 A PCA based on patient's age, aortic diameter, aortic pulse pressure, extensional stiffness
259 and WSS showed no separation of BAV ATAAs from TAV ATAAs (see Fig. 7). However, the
260 loading plot revealed that the most important variables responsible for differences between
261 BAV ATAAs and TAV ATAAs are the pulsed pressure and the patient's age.

262

263 **Discussion**

264 This study aimed to investigate the patterns of extensional stiffness from in vivo dynamic
265 imaging of ATAAs and to evaluate potential correlations with clinical data and blood shear
266 forces. The extensional stiffness did not show any significant difference between BAV ATAAs
267 and TAV ATAAs. This supports recent evidence and observations for which there should be
268 no distinction in the surgical management of BAV patients versus TAV patients (Agnese et
269 al., 2019). Recently, we performed equibiaxial mechanical testing on ascending aortic tissues
270 with either BAV or TAV (Di Giuseppe et al., 2019) and found no difference in the mean
271 values of the aortic tissue stiffness between BAV ATAAs and TAV ATAAs as reported here.
272 However, other groups who performed mechanical testing on ascending aortic tissues found
273 differences in the mean values of the aortic tissue stiffness between BAV patients and TAV
274 patients (Choudhury et al., 2009; Duprey et al., 2010; Okamoto et al., 2002; Pham et al.,
275 2013; Pichamuthu et al., 2013). We did not measure the extensional stiffness in non
276 aneurysmatic subjects as healthy subjects cannot undergo CT scans. However the stiffness
277 of healthy aortas was measured by a variety of other techniques in the literature and values
278 in a range between 150 kPa and 1000 kPa were reported, with ATAA exhibiting generally a
279 higher stiffness than healthy aortas (Azadani et al., 2013; Walraevens et al., 2008).

280

281 The correlation of patients' age with the extensional stiffness obtained by the LESI
282 methodology was strongly affected by the valve phenotype. For TAV patients, the

283 extensional stiffness did not vary with the patient age but increased with the age of BAV
284 patients. This is likely a consequence of the significant difference in the age of BAV versus
285 TAV patients. Indeed, TAV ATAAs were older than 50 years while most of patients with BAV
286 were <50 years. We also found that BAV ATAAs can be divided into two subgroups: 1)
287 patients younger than 50 years old who had a relatively low extensional stiffness, 2) patients
288 older than 55 years old who had a relatively high extensional stiffness. Martin et al. (Martin et
289 al., 2013b) showed that the biomechanical properties of dilated ascending aorta change
290 between 50 and 60 years, and this could explain either the difference in the extensional
291 stiffness of two subgroups of BAV ATAAs or the lack of correlation between the extensional
292 stiffness and patient age for TAV ATAAs.

293

294 As expected, no significant correlation was found between extensional stiffness and shear
295 stress for Major, Minor and Anterior quadrant, thereby suggesting there is no direct link
296 between hemodynamics and biomechanical properties of ATAA wall. For the posterior
297 quadrant, instead, a significant correlation was observed.

298

299 The extensional stiffness was significantly correlated with both the pulsed pressure and the
300 circumferential strain and stress. Although these variables are directly involved in the
301 derivation of the aortic stiffness in the LESI methodology, these significant correlations can
302 also be interpreted with physiological principles.

303 Relations between the aortic stiffness and the pulsed pressure have been known for
304 decades. Indeed, as the aorta becomes stiffer, the central pulsed pressure is higher due to
305 the increase in the pulse wave velocity and the early return of reflected waves to the heart
306 from following junctions (Fung, 1998). In a young and healthy aorta, the reflected wave tends
307 to hit the aortic root during diastole, serving to increase diastolic pressure and hence
308 improving perfusion of coronary arteries. In aged and stiffened aortas, the reflected hits the
309 aortic root earlier, increasing the systolic pressure and decreasing the diastolic one. The
310 amplitude of reflected waves increases as the arterial stiffness increases, further augmenting

311 central systolic pressure (Chirinos and Segers, 2010a, b; Fung, 1998; Laurent et al., 2005;
312 Mackenzie et al., 2002; O'Rourke and Nichols, 2005). The effects of this supplemental load
313 onto the aorta, which are direct expressions of the stiffness increase, should be reckoned for
314 estimating the risk of rupture or dissection of ATAAs.

315 As expected, the extensional stiffness was also significantly correlated to the circumferential
316 strain since circumferential strains are a direct expression of the aortic stiffness. Stiffening
317 often triggers degradation and/or loss of a fraction of elastin fibers, leading to a reduction of
318 the wall extensibility (Sokolis et al., 2012). Another consequence is also a decrease of the
319 axial stretch of the aorta, producing an increase of the aortic arch curvature named unfolding
320 (Redheuil et al., 2011). The degradation of protein networks in the extracellular matrix of
321 ATAAs can be explained by the unbalance between protein synthesis by vascular cells and
322 protein destruction by matrix metalloproteases (MMPs) (LeMaire et al., 2005). In the cohort
323 from which this study group was extracted, we found that the expression level of MMP-9 is
324 altered in BAV ATAAs vs TAV ATAAs (Gallo et al., 2018). The significant correlation between
325 extensional stiffness and stress is very common for fibrous soft tissues, owing to their
326 exponential stress-strain curve (García-Herrera et al., 2012). This reflects reorientation and
327 straightening of collagen bundles upon loading (Sokolis et al., 2006).

328 When analyzing BAV and TAV ATAAs together, the PCA analysis suggested that BAV
329 ATAAs are likely forming a cluster in the lower quadrants of the multivariate score plot in the
330 direction of the loading associated to patient age. This is not surprising because BAV
331 patients are known to commonly develop ATAA at younger age than TAV (Agnese et al.,
332 2019; LeMaire et al., 2005).

333

334 **Limitations**

335 The LESI approach relies on local equilibrium equations as it is based on the principle of
336 virtual work (Bersi et al., 2016). As for the generalized Laplace's law, the LESI approach
337 considers the local equilibrium between pressures and tensions in a membrane, indicating
338 that the aortic wall experience no shear through the thickness. This may not be a realistic

339 assumption in regions near the aortic branches but these were excluded from the analysis.
340 The peripheral pulsed pressure rather than central aortic pressure was used. However, the
341 mismatch of aortic compliance between the brachial artery and the aorta should be likely
342 reduced or even reversed with the advanced age of our patients. The effect of brachial blood
343 pressure on the extensional stiffness evaluations will be likely minimal in this study.
344 Validation of in silico modeling has to be established. A large sample size including BAV
345 ATAAs matched with the age of TAV ATAAs would be ideal to confirm observations.
346 Unfortunately, we could not compare results with those relative of non aneurysmatic subjects
347 because healthy control volunteers are not allowed to undertake multiphase gated CT scans
348 due to x-ray radiations risks. We are trying to extend our methodology to other imaging
349 modalities (ultrasounds, MRI).

350

351 **Conclusions**

352 We evaluated the patterns of extensional stiffness from the in vivo imaging of ATAAs on a
353 cohort of 30 patients using the LESI methodology. We found no appreciable differences
354 between BAV and TAV patients. Regional differences appeared marginal due to inter-
355 individual variability. The correlation of patients' age with the extensional stiffness strongly
356 depended on the valve phenotype. Strong relationship of the extensional stiffness with the
357 pulsed pressure was found, supported by biomechanical explanations.

358

359 **Acknowledgments**

360 Stéphane Avril is grateful to the European Research Council (ERC grant Biolochanics, grant
361 number 647067) for financial support. This work was supported by a "Ricerca Finalizzata" grant
362 from the Italian Ministry of Health (GR-2011-02348129) to Salvatore Pasta, and by grant from
363 PON FSE-FESR Ricerca Innovazione 2014–2020 to Marzio Di Giuseppe.

364

365 **Conflict of interest statement**

366 The authors confirm there are not conflict of interest associated with this publication.

367

368

369 **Reference**

370 Agnese, V., Pasta, S., Michelena, H.I., Minà, C., Romano, G.M., Carerj, S., Zito, C., Maalouf, J.F., Foley,
371 T.A., Raffa, G., Clemenza, F., Pilato, M., Bellavia, D., 2019. Patterns of ascending aortic dilatation and
372 predictors of surgical replacement of the aorta: A comparison of bicuspid and tricuspid aortic valve
373 patients over eight years of follow-up. *Journal of Molecular and Cellular Cardiology* 135, 31-39.

374

375 Antiga, L., Steinman, D.A., 2004. Robust and objective decomposition and mapping of bifurcating
376 vessels. *IEEE Transactions on Medical Imaging* 23, 704-713.

377

378 Azadani, A.N., Chitsaz, S., Mannion, A., Mookhoek, A., Wisneski, A., Guccione, J.M., Hope, M.D., Ge, L.,
379 Tseng, E.E., 2013. Biomechanical properties of human ascending thoracic aortic aneurysms. *The Annals*
380 *of Thoracic Surgery* 96, 50-58.

381

382 Bersi, M.R., Bellini, C., Di Achille, P., Humphrey, J.D., Genovese, K., Avril, S., 2016. Novel methodology
383 for characterizing regional variations in the material properties of murine aortas. *Journal of*
384 *Biomechanical Engineering* 138, 071005.

385

386 Borger, M.A., Fedak, P.W.M., Stephens, E.H., Gleason, T.G., Girdauskas, E., Ikonomidis, J.S.,
387 Khojnejhad, A., Siu, S.C., Verma, S., Hope, M.D., Cameron, D.E., Hammer, D.F., Coselli, J.S., Moon,
388 M.R., Sundt, T.M., Barker, A.J., Markl, M., Della Corte, A., Michelena, H.I., Elefteriades, J.A., 2018. The
389 american association for thoracic surgery consensus guidelines on bicuspid aortic valve-related
390 aortopathy: full online-only version. *The Journal of Thoracic and Cardiovascular Surgery* 156, e41-e74.

391

392 Chirinos, J.A., Segers, P., 2010a. Noninvasive evaluation of left ventricular afterload: part 1: pressure
393 and flow measurements and basic principles of wave conduction and reflection. *Hypertension* 56, 555-
394 562.

395

396 Chirinos, J.A., Segers, P., 2010b. Noninvasive evaluation of left ventricular afterload: part 2: arterial
397 pressure-flow and pressure-volume relations in humans. *Hypertension* 56, 563-570.

398

399 Choudhury, N., Bouchot, O., Rouleau, L., Tremblay, D., Cartier, R., Butany, J., Mongrain, R., Leask, R.L.,
400 2009. Local mechanical and structural properties of healthy and diseased human ascending aorta
401 tissue. *Cardiovascular Pathology* 18, 83-91.

402

403 Coady, M.A., Rizzo, J.A., Goldstein, L.J., Elefteriades, J.A., 1999. Natural history, pathogenesis and
404 etiology of thoracic aortic aneurysms and dissections. *Cardiology Clinics* 17, 615-635.

405

406 D'Ancona, G., Amaducci, A., Rinaudo, A., Pasta, S., Follis, F., Pilato, M., Baglini, R., 2013. Haemodynamic
407 predictors of a penetrating atherosclerotic ulcer rupture using fluid-structure interaction analysis.
408 *Interactive Cardiovascular and Thoracic Surgery* 17, 576-578.

409

410 Di Giuseppe, M., Alotta, G., Agnese, V., Bellavia, D., Raffa, G.M., Vetri, V., Zingales, M., Pasta, S., Pilato,
411 M., 2019. Identification of circumferential regional heterogeneity of ascending thoracic aneurysmal
412 aorta by biaxial mechanical testing. *Journal of Molecular and Cellular Cardiology* 130, 205-215.

413

414 Duprey, A., Khanafer, K., Schlicht, M., Avril, S., Williams, D., Berguer, R., 2010. In vitro characterisation
415 of physiological and maximum elastic modulus of ascending thoracic aortic aneurysms using uniaxial
416 tensile testing. *European Journal of Vascular and Endovascular Surgery* 39, 700-707.
417
418 Duprey, A., Trabelsi, O., Vola, M., Favre, J.-P., Avril, S., 2016. Biaxial rupture properties of ascending
419 thoracic aortic aneurysms. *Acta Biomaterialia* 42, 273-285.
420
421 Elefteriades, J.A., Farkas, E.A., 2010. Thoracic aortic aneurysm: clinically pertinent controversies and
422 uncertainties. *Journal of the American College of Cardiology* 55, 841-857.
423 Farzaneh, S., Trabelsi, O., Avril, S., 2019a. Inverse identification of local stiffness across ascending
424 thoracic aortic aneurysms. *Biomechanics and Modeling in Mechanobiology* 18, 137-153.
425
426 Farzaneh, S., Trabelsi, O., Chavent, B., Avril, S., 2019b. Identifying local arterial stiffness to assess the
427 risk of rupture of ascending thoracic aortic aneurysms. *Annals of Biomedical Engineering* 47, 1038-
428 1050.
429
430 Fung, Y.-C., 1998. *Biomechanics: circulation*. Springer 9, 155.
431
432 Gallo, A., Agnese, V., Coronello, C., Raffa, G.M., Bellavia, D., Conaldi, P.G., Pilato, M., Pasta, S., 2018.
433 On the prospect of serum exosomal miRNA profiling and protein biomarkers for the diagnosis of
434 ascending aortic dilatation in patients with bicuspid and tricuspid aortic valve. *International Journal of*
435 *Cardiology* 273, 230-236.
436
437 García-Herrera, C.M., Atienza, J., Rojo, F., Claes, E., Guinea, G., Celentano, D.J., García-Montero, C.,
438 Burgos, R., 2012. Mechanical behaviour and rupture of normal and pathological human ascending
439 aortic wall. *Medical & Biological Engineering & Computing* 50, 559-566.
440
441 Guala, A., Rodriguez-Palomares, J., Dux-Santoy, L., Teixido-Tura, G., Maldonado, G., Galian, L., Huguet,
442 M., Valente, F., Gutiérrez, L., González-Alujas, T., 2019. Influence of aortic dilation on the regional
443 aortic stiffness of bicuspid aortic valve assessed by 4-dimensional flow cardiac magnetic resonance:
444 comparison with Marfan syndrome and degenerative aortic aneurysm. *JACC: Cardiovascular Imaging*
445 12, 1020-1029.
446
447 Januzzi, J.L., Isselbacher, E.M., Fattori, R., Cooper, J.V., Smith, D.E., Fang, J., Eagle, K.A., Mehta, R.H.,
448 Nienaber, C.A., Pape, L.A., 2004. Characterizing the young patient with aortic dissection: results from
449 the international registry of aortic dissection (IRAD). *Journal of the American College of Cardiology* 43,
450 665-669.
451
452 Joldes, G.R., Miller, K., Wittek, A., Doyle, B., 2016. A simple, effective and clinically applicable method
453 to compute abdominal aortic aneurysm wall stress. *Journal of the Mechanical Behavior of Biomedical*
454 *Materials* 58, 139-148.
455
456 Khanafer, K.M., Gadhoke, P., Berguer, R., Bull, J.L., 2006. Modeling pulsatile flow in aortic aneurysms:
457 effect of non-Newtonian properties of blood. *Biorheology* 43, 661-679.
458
459 Laurent, S., Boutouyrie, P., Lacolley, P., 2005. Structural and genetic bases of arterial stiffness.
460 *Hypertension* 45, 1050-1055.
461
462 LeMaire, S.A., Wang, X., Wilks, J.A., Carter, S.A., Wen, S., Won, T., Leonardelli, D., Anand, G., Conklin,
463 L.D., Wang, X.L., 2005. Matrix metalloproteinases in ascending aortic aneurysms: Bicuspid versus
464 trileaflet aortic valves. *Journal of Surgical Research* 123, 40-48.
465

466 Leuprecht, A., Perktold, K., 2001. Computer simulation of non-Newtonian effects on blood flow in large
467 arteries. *Computer Methods in Biomechanics and Biomedical Engineering* 4, 149-163.
468

469 Longobardo, L., Carerj, M.L., Pizzino, G., Bitto, A., Piccione, M.C., Zucco, M., Oreto, L., Todaro, M.C.,
470 Calabrò, M.P., Squadrito, F., Di Bella, G., Oreto, G., Khandheria, B.K., Carerj, S., Zito, C., 2017.
471 Impairment of elastic properties of the aorta in bicuspid aortic valve: relationship between
472 biomolecular and aortic strain patterns. *European Heart Journal - Cardiovascular Imaging* 19, 879-887.
473 Mackenzie, I., Wilkinson, I., Cockcroft, J., 2002. Assessment of arterial stiffness in clinical practice. *Qjm*
474 95, 67-74.
475

476 Mahadevia, R., Barker, A.J., Schnell, S., Entezari, P., Kansal, P., Fedak, P.W., Malaisrie, S.C., McCarthy,
477 P., Collins, J., Carr, J., 2014. Bicuspid aortic cusp fusion morphology alters aortic three-dimensional
478 outflow patterns, wall shear stress, and expression of aortopathy. *Circulation* 129, 673-682.
479

480 Martin, C., Sun, W., Pham, T., Elefteriades, J., 2013a. Predictive biomechanical analysis of ascending
481 aortic aneurysm rupture potential. *Acta Biomaterialia* 9, 9392-9400.
482

483 Martin, C., Sun, W., Primiano, C., McKay, R., Elefteriades, J., 2013b. Age-dependent ascending aorta
484 mechanics assessed through multiphase CT. *Annals of Biomedical Engineering* 41, 2565-2574.
485

486 Mendez, V., Di Giuseppe, M., Pasta, S., 2018. Comparison of hemodynamic and structural indices of
487 ascending thoracic aortic aneurysm as predicted by 2-way FSI, CFD rigid wall simulation and patient-
488 specific displacement-based FEA. *Computers in Biology and Medicine* 100, 221-229.
489

490 Mousavi, S.J., Avril, S., 2017. Patient-specific stress analyses in the ascending thoracic aorta using a
491 finite-element implementation of the constrained mixture theory. *Biomechanics and Modeling in*
492 *Mechanobiology* 16, 1765-1777.
493

494 O'Rourke, M.F., Nichols, W.W., 2005. Aortic diameter, aortic stiffness, and wave reflection increase
495 with age and isolated systolic hypertension. *Hypertension* 45, 652-658.
496

497 Okamoto, R.J., Wagenseil, J.E., DeLong, W.R., Peterson, S.J., Kouchoukos, N.T., Sundt, T.M., 3rd, 2002.
498 Mechanical properties of dilated human ascending aorta. *Annals of Biomedical Engineering* 30, 624-
499 635.
500

501 Pape, L.A., Tsai, T.T., Isselbacher, E.M., Oh, J.K., O'Gara P, T., Evangelista, A., Fattori, R., Meinhardt, G.,
502 Trimarchi, S., Bossone, E., Suzuki, T., Cooper, J.V., Froehlich, J.B., Nienaber, C.A., Eagle, K.A., 2007.
503 Aortic diameter ≥ 5.5 cm is not a good predictor of type A aortic dissection: observations from the
504 International Registry of Acute Aortic Dissection (IRAD). *Circulation* 116, 1120-1127.
505

506 Pasta, S., Agnese, V., Di Giuseppe, M., Gentile, G., Raffa, G.M., Bellavia, D., Pilato, M., 2017a. In vivo
507 strain analysis of dilated ascending thoracic aorta by ECG-gated CT angiographic imaging. *Annals of*
508 *Biomedical Engineering* 45, 2911-2920.
509

510 Pasta, S., Gentile, G., Raffa, G., Bellavia, D., Chiarello, G., Liotta, R., Luca, A., Scardulla, C., Pilato, M.,
511 2017b. In silico shear and intramural stresses are linked to aortic valve morphology in dilated ascending
512 aorta. *European Journal of Vascular and Endovascular Surgery* 54, 254-263.
513

514 Pham, T., Martin, C., Elefteriades, J., Sun, W., 2013. Biomechanical characterization of ascending aortic
515 aneurysm with concomitant bicuspid aortic valve and bovine aortic arch. *Acta Biomaterialia* 9, 7927-
516 7936.
517

518 Pichamuthu, J.E., Phillippi, J.A., Cleary, D.A., Chew, D.W., Hempel, J., Vorp, D.A., Gleason, T.G., 2013.
519 Differential tensile strength and collagen composition in ascending aortic aneurysms by aortic valve
520 phenotype. *Annals of Thoracic Surgery* 96, 2147-2154.
521
522 Prakash, A., Adlakhia, H., Rabideau, N., Hass, C.J., Morris, S.A., Geva, T., Gauvreau, K., Singh, M.N., Lacro,
523 R.V., 2015. Segmental aortic stiffness in children and young adults with connective tissue disorders:
524 relationships with age, aortic size, rate of dilation, and surgical root replacement. *Circulation* 132, 595-
525 602.
526
527 Raaz, U., Zöllner, A.M., Schellinger, I.N., Toh, R., Nakagami, F., Brandt, M., Emrich, F.C., Kayama, Y.,
528 Eken, S., Adam, M., 2015. Segmental aortic stiffening contributes to experimental abdominal aortic
529 aneurysm development. *Circulation* 131, 1783-1795.
530
531 Redheuil, A., Yu, W.-C., Mousseaux, E., Harouni, A.A., Kachenoura, N., Wu, C.O., Bluemke, D., Lima,
532 J.A.C., 2011. Age-related changes in aortic arch geometry: relationship with proximal aortic function
533 and left ventricular mass and remodeling. *Journal of the American College of Cardiology* 58, 1262-1270.
534
535 Rooprai, J., Boodhwani, M., Beauchesne, L., Chan, K.L., Dennie, C., Nagpal, S., Messika-Zeitoun, D.,
536 Coutinho, T., 2019. Thoracic aortic aneurysm growth in bicuspid aortic valve patients: role of aortic
537 stiffness and pulsatile hemodynamics. *Journal of the American Heart Association* 8, e010885.
538
539 Selvin, E., Najjar, S.S., Cornish, T.C., Halushka, M.K., 2010. A comprehensive histopathological
540 evaluation of vascular medial fibrosis: Insights into the pathophysiology of arterial stiffening.
541 *Atherosclerosis* 208, 69-74.
542
543 Smoljkic, M., Fehervary, H., Van den Bergh, P., Jorge-Penas, A., Kluyskens, L., Dymarkowski, S.,
544 Verbrugge, P., Meuris, B., Vander Sloten, J., Famaey, N., 2017. Biomechanical characterization of
545 ascending aortic aneurysms. *Biomechanics and Modeling in Mechanobiology* 16, 705-720.
546
547 Sokolis, D.P., Kefaloyannis, E.M., Kouloukoussa, M., Marinos, E., Boudoulas, H., Karayannacos, P.E.,
548 2006. A structural basis for the aortic stress–strain relation in uniaxial tension. *Journal of Biomechanics*
549 39, 1651-1662.
550
551 Sokolis, D.P., Kritharis, E.P., Giagini, A.T., Lampropoulos, K.M., Papadodima, S.A., Iliopoulos, D.C., 2012.
552 Biomechanical response of ascending thoracic aortic aneurysms: association with structural
553 remodelling. *Computer Methods in Biomechanics and Biomedical Engineering* 15, 231-248.
554
555 Sulejmani, F., Pokutta-Paskaleva, A., Ziganshin, B., Leshnower, B., Iannucci, G., Elefteriades, J., Sun, W.,
556 2017. Biomechanical properties of the thoracic aorta in Marfan patients. *Annals of Cardiothoracic*
557 *Surgery* 6, 610.
558
559 Teixeira, R., Moreira, N., Baptista, R., Barbosa, A., Martins, R., Castro, G., Providência, L., 2012.
560 Circumferential ascending aortic strain and aortic stenosis. *European Heart Journal - Cardiovascular*
561 *Imaging* 14, 631-641.
562
563 van Ooij, P., Markl, M., Collins, J.D., Carr, J.C., Rigsby, C., Bonow, R.O., Malaisrie, S.C., McCarthy, P.M.,
564 Fedak, P.W., Barker, A.J., 2017. Aortic valve stenosis alters expression of regional aortic wall shear
565 stress: New insights from a 4-dimensional flow magnetic resonance imaging study of 571 subjects.
566 *Journal of the American Heart Association* 6, e005959.
567
568 Verma, S., Siu, S.C., 2014. Aortic dilatation in patients with bicuspid aortic valve. *New England Journal*
569 *of Medicine* 370, 1920-1929.

570
571 Walraevens, J., Willaert, B., De Win, G., Ranftl, A., De Schutter, J., Vander Sloten, J., 2008. Correlation
572 between compression, tensile and tearing tests on healthy and calcified aortic tissues. *Medical*
573 *Engineering & Physics* 30, 1098-1104.
574 Youssefi, P., Gomez, A., He, T., Anderson, L., Bunce, N., Sharma, R., Figueroa, C.A., Jahangiri, M., 2017.
575 Patient-specific computational fluid dynamics—assessment of aortic hemodynamics in a spectrum of
576 aortic valve pathologies. *The Journal of Thoracic and Cardiovascular Surgery* 153, 8-20. e23.

577

578

579

580

581

582

583

584

585

586

587

588

589

590

591

592

593

594

595

596

597

598

599 **Figure Legends**

600 **Figure 1:** Representation of ATAA: anterior, posterior, major and minor regions are shown in
601 boxes.

602 **Figure 2:** Representative extensional stiffness maps of 6 patients reconstructed using LESI
603 methodology for TAV ATAA and BAV ATAA patients.

604 **Figure 3:** Representative wall shear stress maps of 2 patients obtained by CFD analysis for
605 TAV ATAA and BAV ATAA patients.

606 **Figure 4:** Comparisons of average extensional stiffness of BAV ATAAs and TAV ATAAs
607 evaluated at different quadrants.

608 **Figure 5:** (A) Correlation between average extensional stiffness and ascending aortic
609 diameter; (B) correlation between average extensional stiffness and aortic pulse pressure;
610 (C) correlation between average extensional stiffness and patients' age of BAV ATAAs; (D)
611 correlation between average extensional stiffness patients' age of TAV ATAAs; (E) average
612 extensional stiffness vs circumferential strain data with regression curve; (F) correlation
613 between average extensional stiffness and circumferential stress.

614 **Figure 6:** Correlation between extensional stiffness and peak systolic WSSs evaluated at
615 proximal ascending aorta from (A) major, (B) minor, (C) anterior and (D) posterior regions.

616 **Figure 7:** Two-dimensional score plots of PC1 versus PC2 with loading showing the main
617 variables responsible for clustering BAV ATAAs (black dots) from TAV ATAAs (red dots); the
618 plot shows patient's age, aortic diameter, aortic pulse pressure, extensional stiffness and wall
619 shear stress. Solid lines represent 95% tolerance ellipse of TAV ATAAs (red color) and BAV
620 ATAAs (black color).

621 **Figure A1:** Correlation between average extensional stiffness vs circumferential strain data
622 with regression curve for BAV (A) and TAV (B) patients; correlation between average
623 extensional stiffness vs circumferential stress for BAV (C) and TAV (D) patients; correlation
624 between average extensional stiffness vs aortic pulse pressure for BAV (E) and TAV (F)
625 patients; correlation between average extensional stiffness vs aortic diameter for BAV (G)
626 and TAV (H) patients.

627 **Figure A2:** Correlation between extensional stiffness and peak systolic WSSs evaluated at
628 proximal ascending aorta from major, minor, anterior and posterior regions for BAV
629 (A,C,E,G) and TAV patients (B,D,F,H).

630

631

632

633

634

635

636

637

638

639

640

641

642

643

644

645

646

647

648

649

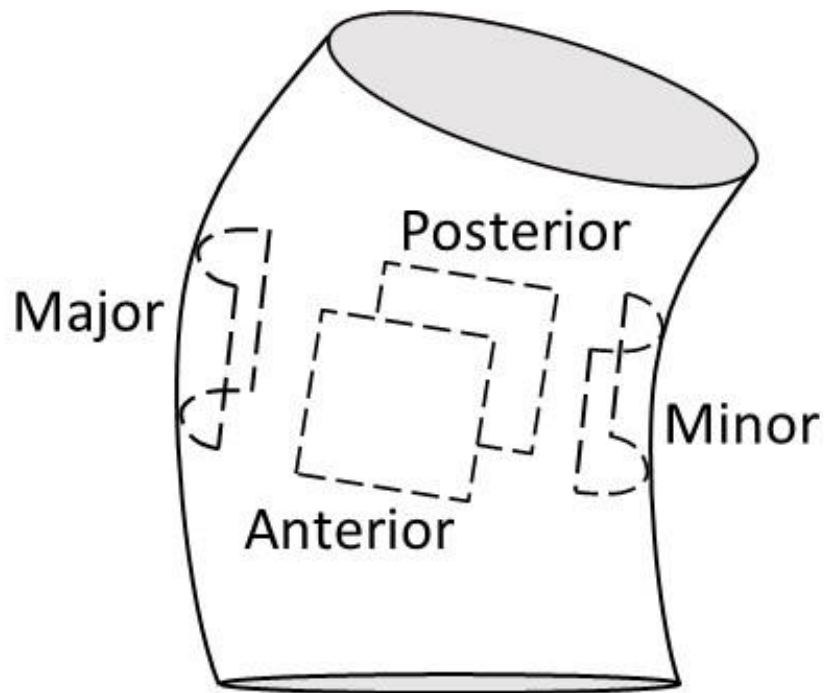
650

651

652

653

654 **Figure 1**



655

656

657

658

659

660

661

662

663

664

665

666

667

668

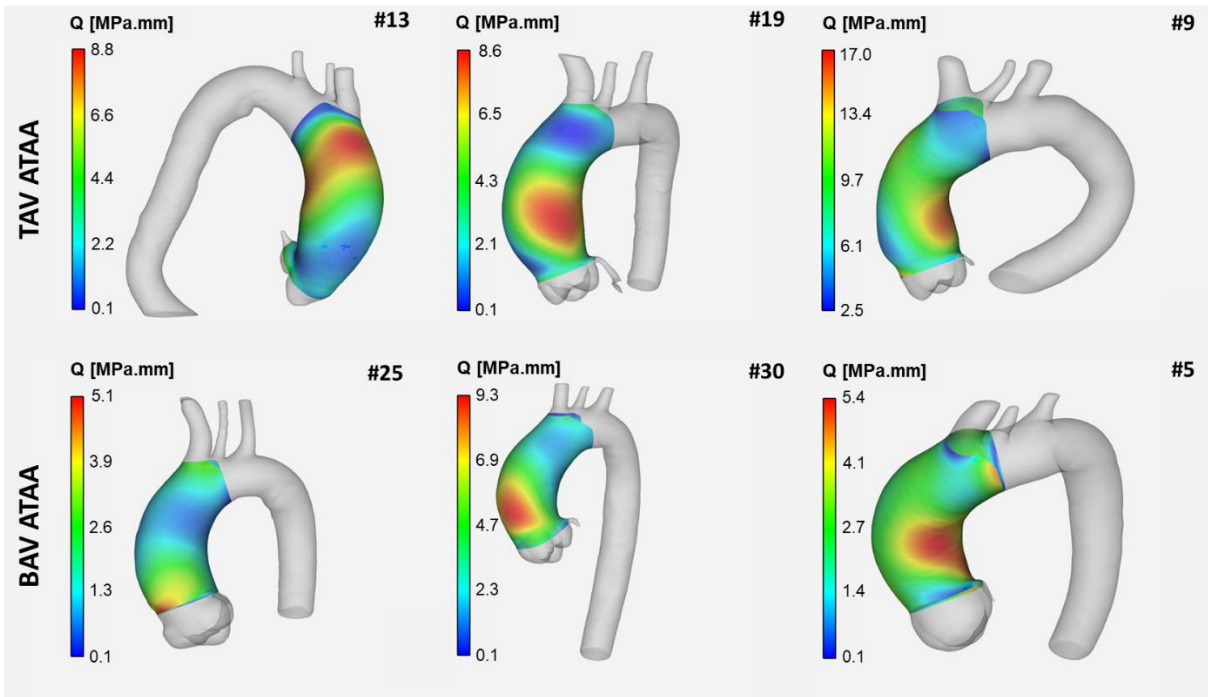
669

670

671

672

673 **Figure 2**



674

675

676

677

678

679

680

681

682

683

684

685

686

687

688

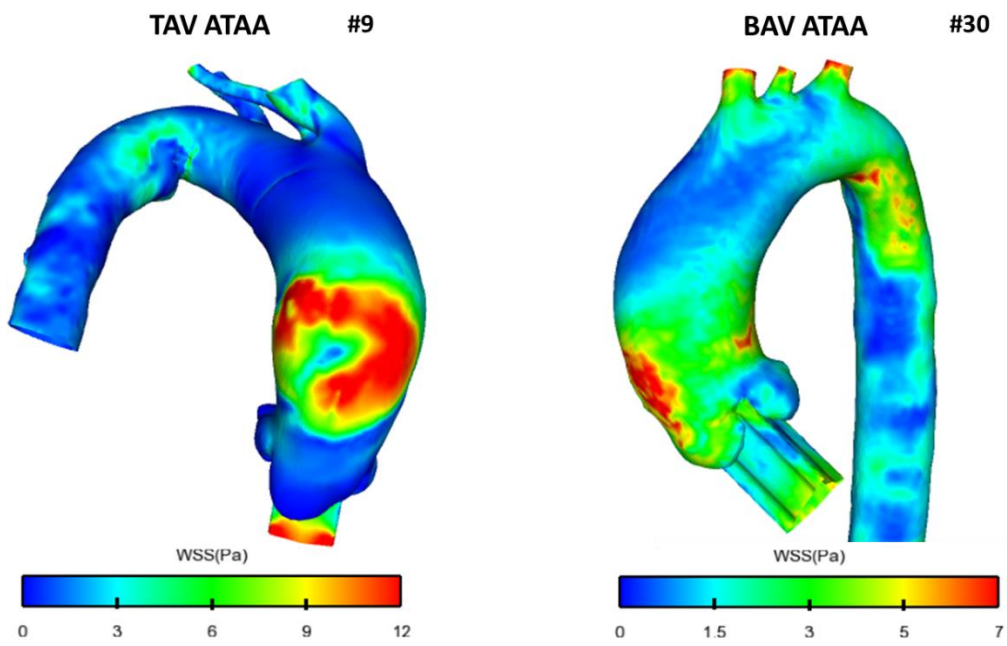
689

690

691

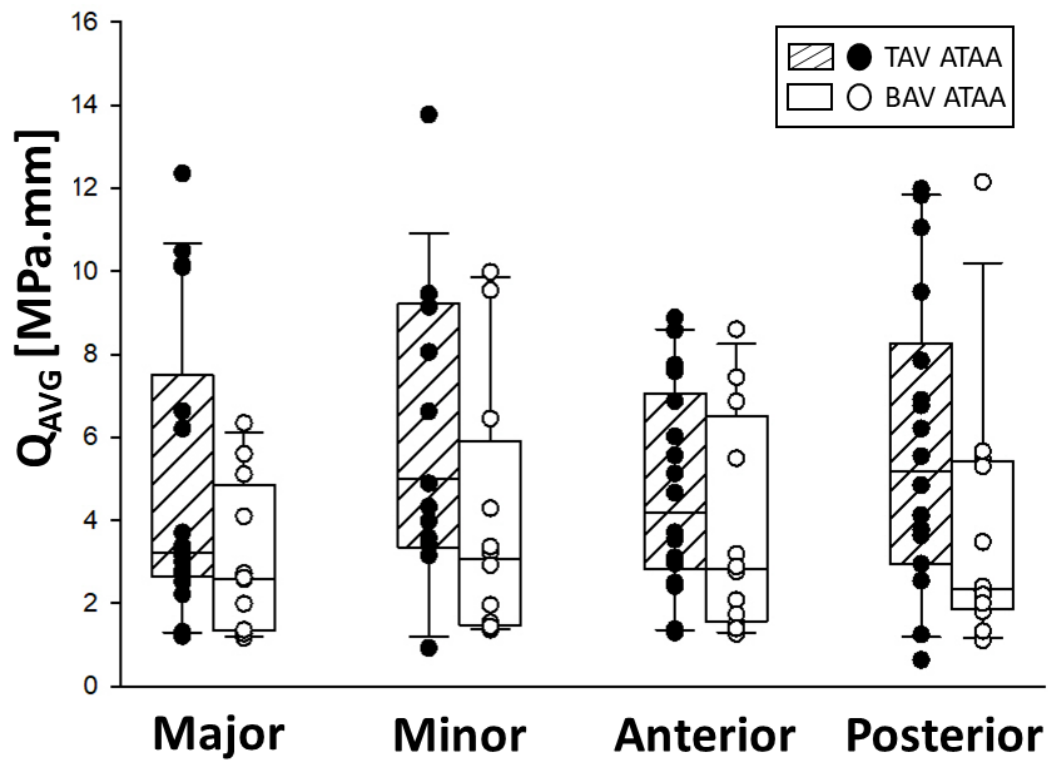
692

693 **Figure 3**



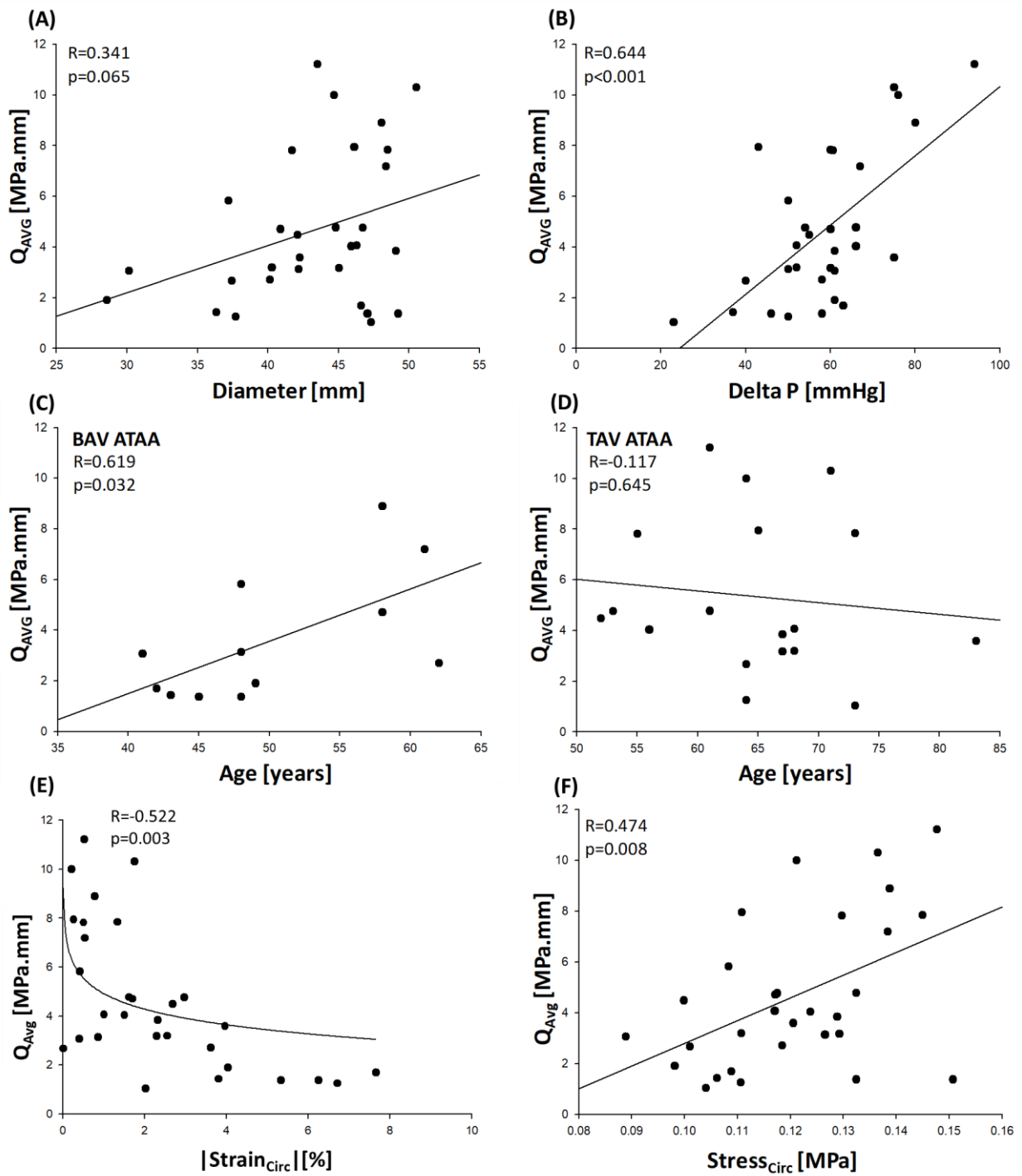
694
695
696
697
698
699
700
701
702
703
704
705
706
707
708
709
710
711

712 **Figure 4**



713
714
715
716
717
718
719
720
721
722
723
724
725
726
727
728

729 **Figure 5**



730

731

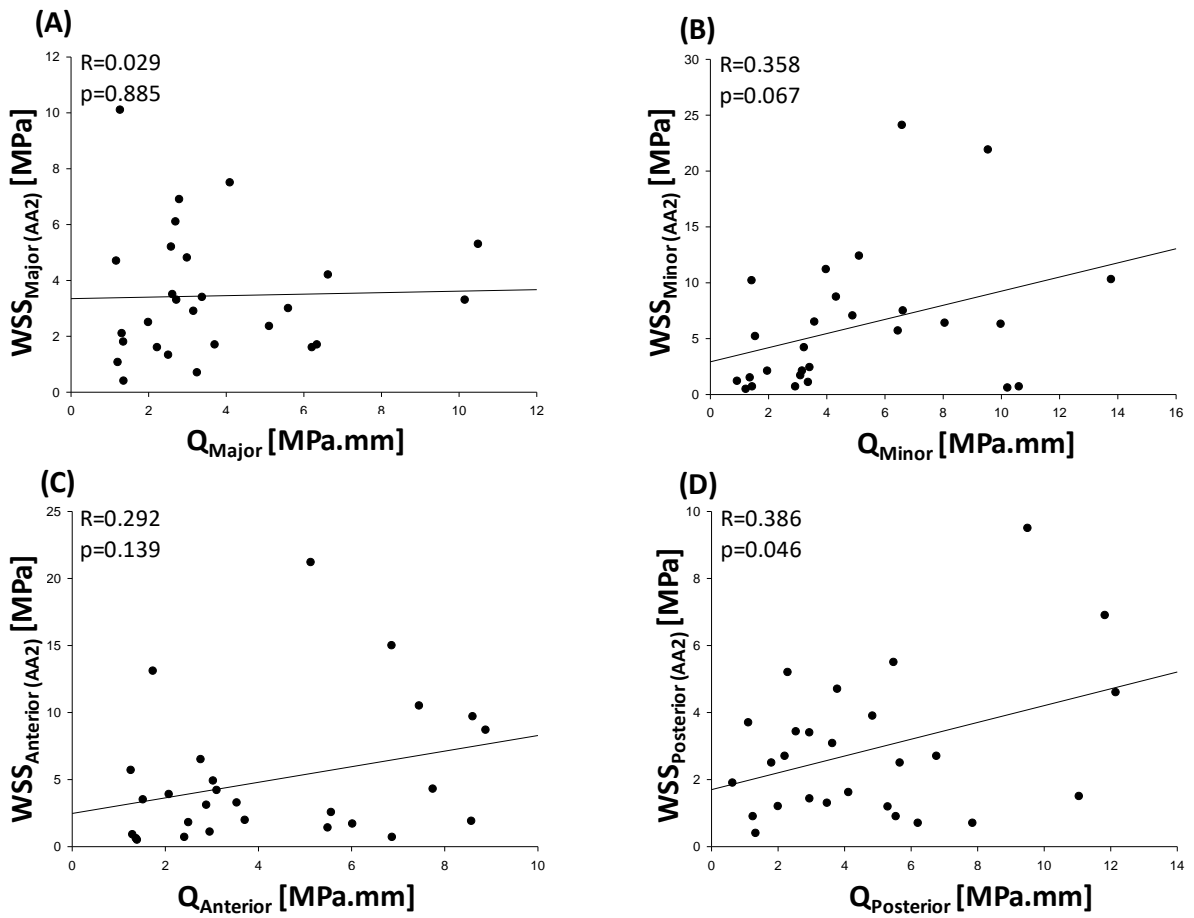
732

733

734

735

736 **Figure 6**



737

738

739

740

741

742

743

744

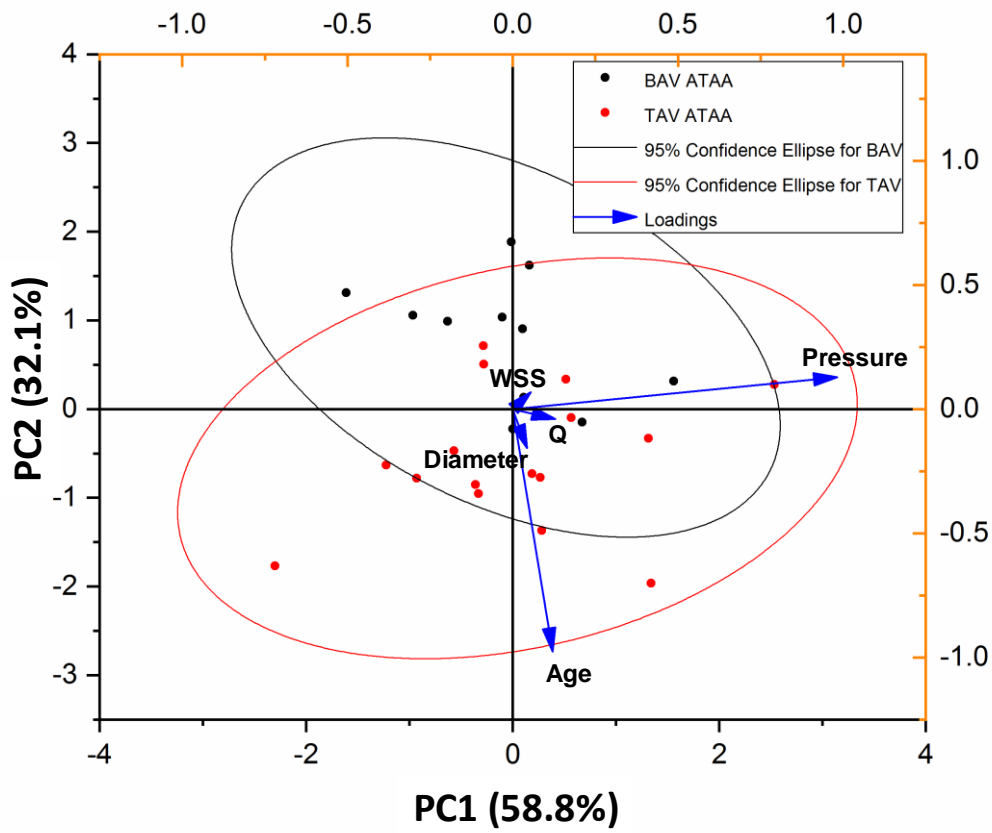
745

746

747

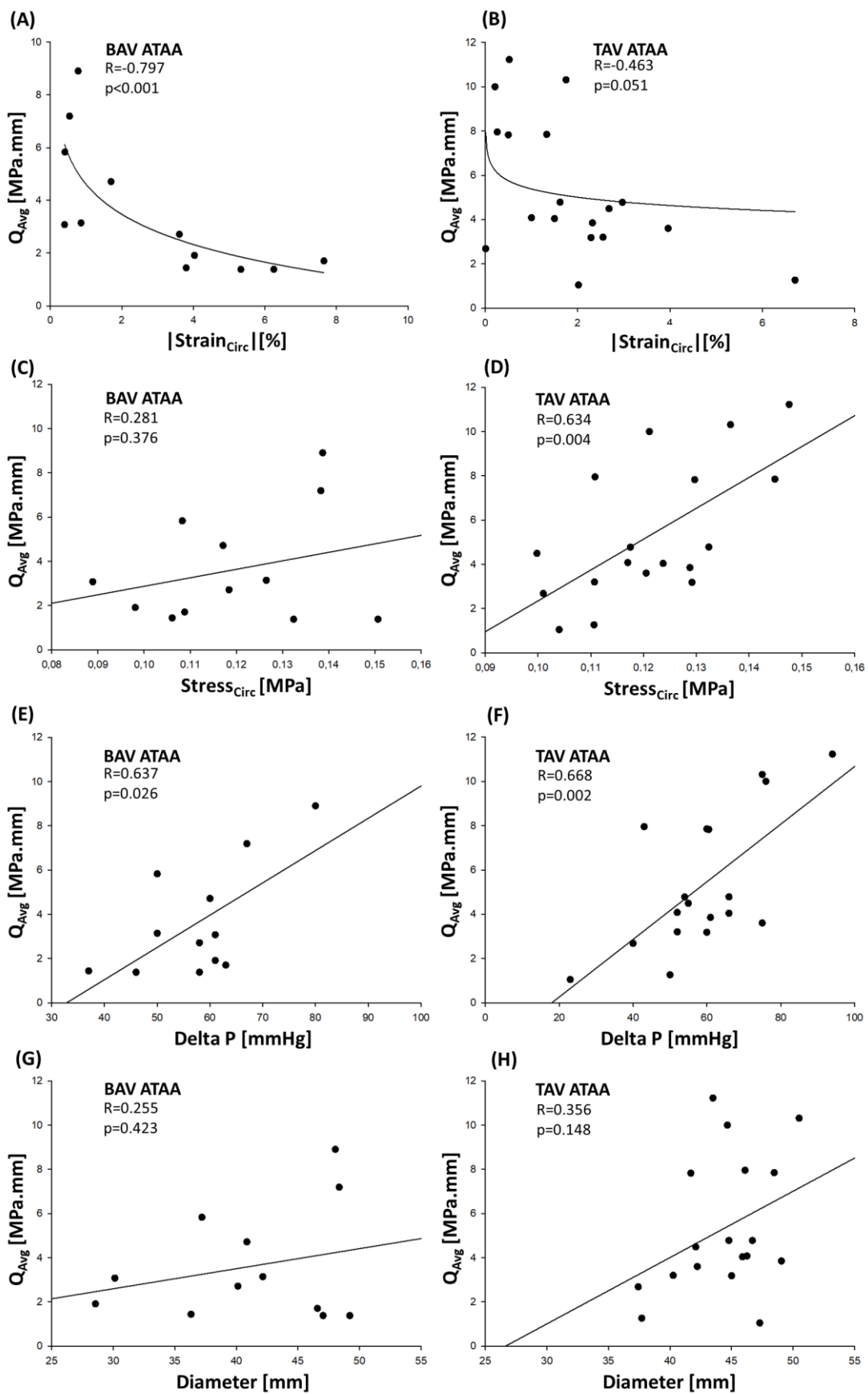
748

749 **Figure 7**

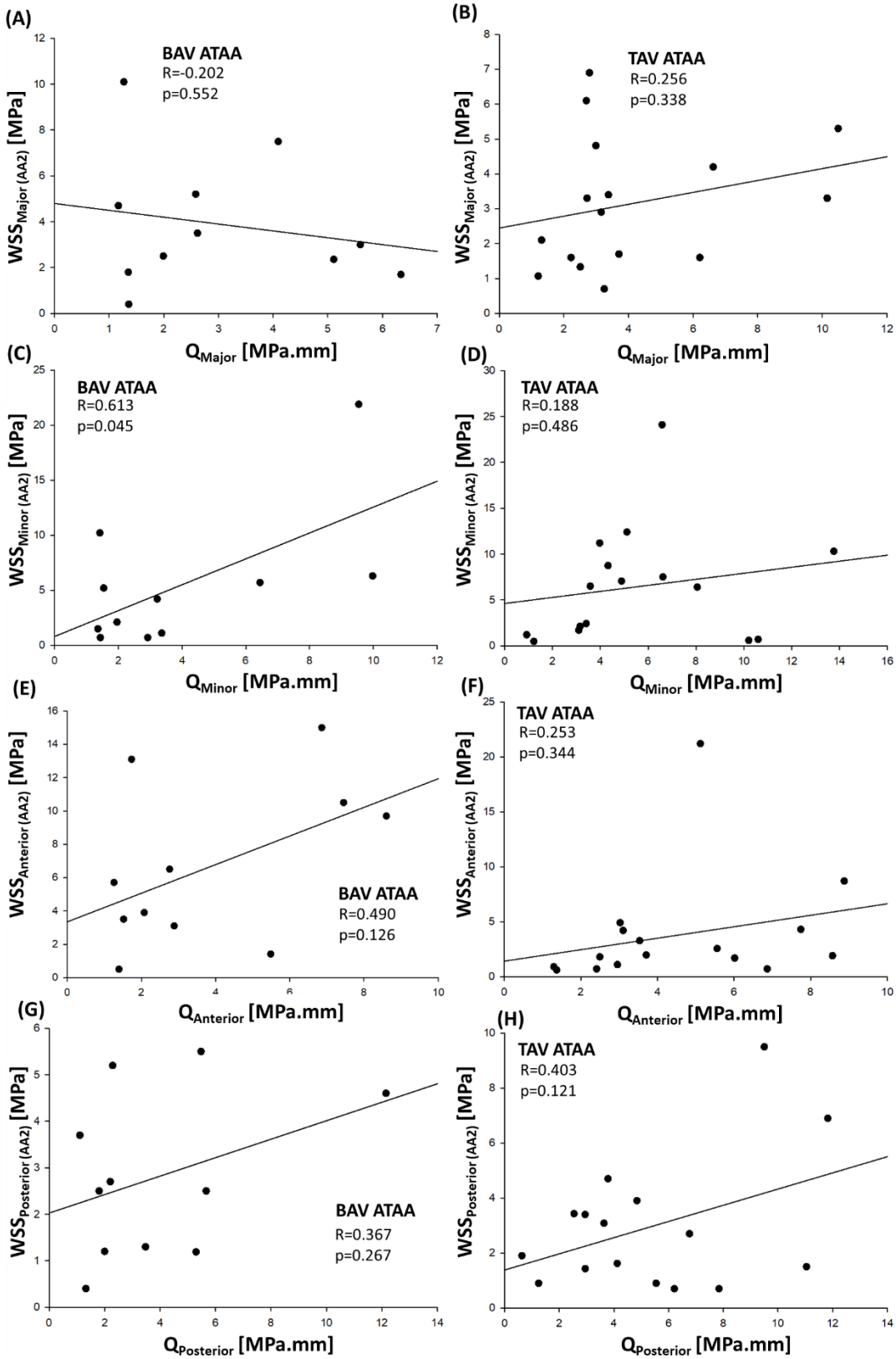


750
751
752
753
754
755
756
757
758
759
760
761
762
763
764

765 **Figure A1**



766



768

769

770

771 **Table 1:** Demographic and clinical data.

ID	Sex	Valve	Age [years]	Systolic Pressure [mmHg]	Diastolic Pressure [mmHg]	Aortic Diameter [mm]
1	M	TAV	56	140	74	45.9
2	M	TAV	55	136	76	41.7
3	M	BAV	62	135	77	40.13
4	M	BAV	43	125	88	36.32
5	M	BAV	48	135	85	42.15
6	M	TAV	71	145	70	50.5
7	M	BAV	58	150	70	48.04
8	M	TAV	73	100	77	47.3
9	M	TAV	61	180	86	43.5
10	M	TAV	67	136	75	49.05
11	M	TAV	67	140	80	45.01
12	M	TAV	68	122	70	46.27
13	F	TAV	83	150	75	42.23
14	M	TAV	65	116	73	46.1
15	M	TAV	61	136	70	44.8
16	M	BAV	48	130	80	37.2
17	M	BAV	49	136	75	28.56
18	M	TAV	68	129	77	40.27
19	M	TAV	53	126	72	46.7
20	F	TAV	64	144	68	44.67
21	M	TAV	73	144	84	48.47
22	M	BAV	41	136	75	30.13
23	M	BAV	42	131	68	46.59
24	M	TAV	64	120	80	37.43
25	M	BAV	48	148	90	47.05
26	M	TAV	64	130	80	37.71
27	M	BAV	45	124	78	49.21
28	F	BAV	61	144	77	48.36
29	F	TAV	52	125	70	42.1
30	M	BAV	58	136	76	40.86
			58.9±10.4	135.0±13.8	76.5±5.8	43.1±5.4

772

773